J|A|C|S
ARTICLES
Published on Web 11/20/2003

Excited-State Metal-to-Ligand Charge Transfer Dynamics of a Ruthenium(II) Dye in Solution and Adsorbed on TiO_2 Nanoparticles from Resonance Raman Spectroscopy

Lian C. T. Shoute and Glen R. Loppnow*

Contribution from the Department of Chemistry, University of Alberta, Edmonton, Alberta, Canada

Received March 19, 2003; E-mail: glen.loppnow@ualberta.ca

Abstract: The dynamics of metal-to-ligand charge transfer (MLCT) in a *cis*-bis(4,4′-dicarboxy-2,2′-bipyridine)-bis(isothiocyanato)ruthenium(II) dye (N3) are compared for the free dye in solution and the dye adsorbed on the surface of the TiO_2 nanoparticles from resonance Raman spectroscopy. The 544-nm MLCT absorption band of N3 adsorbed on TiO_2 is slightly blue-shifted from that of the free N3, indicating a weak electronic coupling between N3 and TiO_2. The resonance Raman spectra of N3 and the N3|TiO_2 complex obtained upon excitation within the lowest-lying MLCT singlet state of the dye are similar except for slight shifts in band positions. Resonance Raman cross sections have been obtained for the vibrational modes of both N3 and N3|TiO_2 with excitation frequencies spanning the 544-nm MLCT band. Self-consistent analysis of the resulting resonance Raman excitation profiles and absorption spectrum using a time-dependent wave packet formalism over two electronic states yields mode-specific vibrational and solvent reorganization energies. Despite the weak electronic coupling between N3 and TiO_2 in N3|TiO_2, adsorption strongly affects the reorganization energies of N3 in the intramolecular MLCT state. Adsorption of N3 onto TiO_2 increases the absolute Raman cross section of each mode by a factor of ca. 1.6 and decreases the vibrational and solvent reorganization energies by factors of 2 and 6, respectively. The excited-state dynamics of N3 adsorbed on the surface of TiO_2 nanoparticles were observed to be independent of the number of N3 molecules adsorbed per TiO_2 nanoparticle. The effect of TiO_2 on the dynamics of the adsorbed N3 is primarily due to both mode-specific vibrational and electronic pure dephasing, with the dominant contribution from the latter process.

Introduction

Dye sensitization is the basis of color photography,[1] electrophotography,[2] and photoelectrochemical cells.[3−10] The photophysics and photochemistry of ruthenium(II)bis(2,2′-bipyridine)-(L_2) dyes and their derivatives are topics of current interest because they have applications as sensitizer dyes in solar-to-electrical energy conversion.[11−18] Interfacial charge-transfer dynamics of these dyes have been extensively investigated by femtosecond time-domain techniques in recent years.[19−28] Photoelectrochemical cells based on ruthenium polypyridyl dye-

(1) (a) Jacobson, K. I.; Jacobson, R. E. *Imaging Systems*, John Wiley & Sons: New York, 1976. (b) Tani, T. J. *Imaging Sci*. **1990**, *34*, 143. (c) Tani, T.; Suzumoto, T.; Ohzeki, K. *J. Phys. Chem.* **1990**, *94*, 1298−1301.
(2) Kiess, H. *Prog. Surf. Sci.* **1997**, *9*, 113.
(3) (a) Hagfeldt, A. Gratzel, M. *Chem. Rev.* **1995**, *95*, 49−68. (b) Hagfeldt, A.; Gratzel, M. *Acc. Chem. Res.* **2000**, *33*, 269−277. (c) O'Regan, B.; Gratzel, M. *Nature* **1991**, *353*, 737−739.
(4) Nazeeruddin, M. K.; Kay, A.; Roficio, I.; Humphry-Baker, R.; Muller, E.; Liska, P.; Vlachopoulos, N.; Gratzel, M. *J. Am. Chem. Soc.* **1993**, *115*, 6382−6390.
(5) Nazeeruddin, M. K.; Pechy, P.; Renouard, T.; Zakeeruddin, S. M.; Humphery-Baker, R.; Comte, P.; Liska, P.; Cevey, L.; Costa, E.; Shklover, V.; Spiccia, L.; Deacon, G. B.; Bignozzi, C. A.; Gratzel, M. *J. Am. Chem. Soc.* **2001**, *123*, 1613−1624.
(6) Ferrere, S.; Gregg, B. A. *J. Phys. Chem. B* **2001**, *105*, 7602−7605.
(7) He, J.; Benko, G.; Korodi, F.; Polivka, T.; Lomoth, R.; Akermark, B.; Sun, L.; Hagfeldt, A.; Sundstrom, V. *J. Am. Chem. Soc.* **2002**, *124*, 4922−4932.
(8) Wang, Z.-S.; Li, F.-Y.; Huang, C.-H. *J. Phys. Chem. B* **2001**, *105*, 9210−9217.
(9) (a) Hara, H.; Sato, T.; Katoh, R.; Furube, A.; Ohga, Y.; Shinpo, A.; Suga, S.; Sayama, K.; Sugihara, H.; Arakawa, H. *J. Phys. Chem. B* **2003**, *107*, 597−606. (b) Yanagida, M.; Islam, A.; Tachibana, Y.; Fujihashi, G.; Katoh, R.; Sugihara, H.; Arakawa, H. *New J. Chem.* **2002**, *26*, 963−965.
(10) (a) Matsumoto, M.; Wada, Y.; Kitamura, T.; Shigaki, K.; Inoue, T.; Ikeda, M.; Yanagida, S. *Bull. Chem. Soc. Jpn.* **2001**, *74*, 387−393. (b) Ito, S.; Ishikawa, K.; Wen, C.-J.; Yoshida, S.; Watanabe, T. *Bull. Chem. Soc. Jpn.* **2000**, *73*, 2609−2614. (c) Stergiopoulos, T.; Arabatzis, I. M.; Katsaros, G.; Falaras, P. *Nanoletters* **2002**, *2*, 1259−1261.
(11) (a) Balzani, V.; Juris, A.; Venturi, M.; Campagna, S.; Serroni, S. *Chem. Rev.* **1996**, *96*, 759−833. (b) Juris, A.; Balzani, V.; Barigelletti, F.; Campagna, S.; Belser, P.; Von Zelewsky, A. *Coord. Chem. Rev.* **1988**, *84*, 85−277. (c) Balzani, V.; Campagna, S.; Denti, G.; Juris, A.; Serroni, S.; Venturi, M. *Acc. Chem. Res.* **1998**, *31*, 26−34.
(12) (a) Meyer, T. J. *Pure Appl. Chem.* **1986**, *58*, 1193−1206. Lumpkin, R. S.; Kober, E. M.; Worl, L. A.; Murtaza, Z.; Meyer, T. J. *J. Phys. Chem.* **1990**, *94*, 239−243. (b) Durham, B.; Caspar, J. V.; Nagle, J. K.; Meyer, T. J. *J. Am. Chem. Soc.* **1982**, *104*, 4803−4810. (c) Crosby, G. A. *Acc. Chem. Res.* **1975**, *8*, 231−238.
(13) (a) Thompson, D. W.; Wishart, J. F.; Brunschwig, B. S.; Sutin, N. *J. Phys. Chem. A* **2001**, *105*, 8117−8122. (b) Ponce, A.; Gray, H. B.; Winkler, J. R. *J. Am. Chem. Soc.* **2000**, *122*, 8187−8191. (c) Rudmann, H.; Shimada, S.; Rubner, M. F. *J. Am. Chem. Soc.* **2002**, *124*, 4918−4921.
(14) Bhashikuttan, A. C.; Suzuki, M.; Nakashima, S.; Okada, T. *J. Am. Chem. Soc.* **2002**, *124*, 8398−8405.
(15) Staffilani, M.; Belser, P.; Hartl, F.; Kleverlaan, C. J.; Cola, L. D. *J. Phys. Chem. A* **2002**, *106*, 9242−9250.
(16) (a) Waterland, M. R.; Kelley, D. F. *J. Phys. Chem. A* **2001**, *105*, 4019−4028. (b) Cushing, J. P.; Butoi, C.; Kelley, D. F. *J. Phys. Chem. A* **1997**, *101*, 7222−7230.
(17) (a) Yeh, A. T.; Shank, C. V.; McCusker, J. K. *Science* **2000**, *289*, 935−938. (b) Damrauer, N. H.; Cerullo, G.; Yeh, A.; Boussie, T. R.; Shank, C. V.; McCusker, J. K. *Science* **1997**, *275*, 54−57. (c) Damrauer, N. H.; McCusker, J. K. *J. Phys. Chem. A* **1999**, *103*, 8440−8446. (d) Monat, J. E.; McCusker, J. K. *J. Am. Chem. Soc.* **2000**, *122*, 4092−4097.
(18) Shaw, G. B.; Brown, C. L.; Papanikolas, J. M. *J. Phys. Chem. A* **2002**, *106*, 1483−1495.

10.1021/ja035231v CCC: $25.00

sensitized TiO_2 nanocrystalline films have high solar-to-electrical energy conversion efficiencies of 10.4% and may become a cost-effective alternative to solid-state photovoltaic cells.[3−5] Such a system provides ultimate control, because both the TiO_2 and dye components can be independently studied and modified at the molecular level to enhance device performance. The dye in these cells plays a crucial role, as it acts as an antenna to harvest solar light and initiates charge separation by injecting electrons into the conduction band continuum of the TiO_2 nanoparticles. Therefore, understanding the excited-state dynamics of the dye is critical to optimize the performance of the device. At present, the use of a *cis*-bis(4,4′-dicarboxy-2,2′-bipyridine)-bis(isothiocyanato)ruthenium(II) dye (N3) or its terpyridyl analogues as the sensitizing dye provides the most efficient TiO_2 based solar cells.[3−5] In contrast to the Ru-polypyridyl dyes, other sensitizers similarly covalently linked to TiO_2 nanoparticles in solar cells have been shown to yield solar-to-electrical energy conversion efficiencies that are significantly lower.[6−9,29] This raises a fundamental question of what factors are responsible for making Ru-polypyridyl dyes superior to other dyes in the functioning of dye-sensitized solar cells?

The intense visible absorption band of N3 dye has been assigned to a metal-to-ligand charge-transfer (MLCT) transition from the t_{2g} d orbitals localized on the Ru metal to π^* orbitals localized on a bipyridine ligand.[4,12a,14,16a,18] Thus, photoexcitation formally leads to oxidation of Ru(II) to Ru(III) and the formation of a bipyridine radical anion. The carboxylate substituents on the bipyridine ligands are covalently bound to the surface Ti(IV) ion of TiO_2, and the possible overlap of the accepting metal d orbitals of the TiO_2 conduction band and the N3 carboxylate π^* orbitals may facilitate rapid electron transfer from the radical anion of bipyridine.

Recently, we have reported[30] a detailed study on the excited-state charge-transfer dynamics of alizarin-sensitized TiO_2 nanoparticles using resonance Raman techniques. Alizarin (Alz) chemisorbed on TiO_2 forms an intense, red-shifted charge-transfer absorption band, and electronic excitation into this band corresponds to electron transfer from the adsorbed alizarin to the conduction band of the semiconductor TiO_2 nanoparticle. Alz|TiO_2 has a small vibrational reorganization energy, smaller than any other vibrational reorganization energy measured to date.[31,32] Moreover, in contrast to molecular based donor−acceptor charge-transfer complexes,[31] the accepting modes of the TiO_2 nanoparticle do not contribute to the vibrational reorganization energy. These results have been attributed[30] to the effects of rapid electronic and/or vibrational dephasing in the TiO_2 nanoparticle, facilitated by the high density of states. However, a quantitative comparison of the dynamics of free alizarin and the Alz|TiO_2 complex could not be made because of the strong fluorescence of uncomplexed alizarin in solution.

In this paper, we compare the excited-state MLCT dynamics in *cis*-bis(4,4′-dicarboxy-2,2′-bipyridine)-bis(isothiocyanato)-ruthenium(II) adsorbed on TiO_2 and free in solution with resonance Raman spectroscopy. The MLCT excited state of N3 emits negligible fluorescence due to ultrafast (70 fs) intersystem crossing and emits weak red-shifted luminescence from the triplet state[3,4,16a,19−26] Therefore, the MLCT transition of N3 provides an opportunity to study the effects of the TiO_2 nanoparticle on the dynamics of electron transfer within the Ru complex by comparing the MLCT excited-state dynamics of N3|TiO_2 and free N3 in solution using resonance Raman spectroscopy. The results show that the absolute Raman scattering cross sections are significantly increased and the reorganization energies are significantly decreased for the adsorbed dye. These differences are discussed in terms of structure and the dephasing mechanisms present when the species are adsorbed on a surface.

Experimental Section

Colloidal nanoparticles of TiO_2 were prepared from $TiCl_4$ (Aldrich, Milwaukee, WI) by a procedure described in the literature.[30,33] No polymer stabilizer was added to the solution. With this procedure, the average diameter of the TiO_2 particles should be in the range of 16 nm, based on earlier studies.[33] N3 dye was purchased from Solaronix SA (Aubonne, Switzerland) and used without further purification. The N3-sensitized TiO_2 nanoparticle was prepared by adding N3 into vigorously stirred colloidal TiO_2 in water. Adsorption onto TiO_2 nanoparticles increases the apparent solubility of N3 in aqueous solution; a suspension-free saturated aqueous solution of N3 is $<4 \times 10^{-5}$ M N3. Adsorption allows the preparation of a solution containing >1 mM N3 adsorbed to TiO_2, depending on the concentration of TiO_2 nanoparticles. For preparation of the N3|TiO_2 complex in neat dimethyl sulfoxide (ACP Chemicals Inc., Georgetown, Ontario, Canada) solvent, the N3|TiO_2 aqueous solution was evaporated in a rotary evaporator, dried in air, and then redissolved in dimethyl sulfoxide (DMSO).

(19) (a) Benko, G.; Kallioinen, J.; Korppi-Tommola, J. E. I.; Yartsev, A. P.; Sundstrom, V. *J. Am. Chem. Soc.* **2002**, *124*, 489−493. (b) Kallioinen, J.; Benko, G.; Sundstrom, V.; Korppi-Tommola, J. E. I.; Yartsev, A. P. *J. Phys. Chem. B* **2002**, *106*, 4396−4404.

(20) (a) Asbury, J. B.; Hao, E.; Wang, Y.; Ghosh, H. N.; Lian, T. *J. Phys. Chem. B* **2001**, *105*, 4545−4557. (b) Asbury, J. B.; Ellingson, R. J.; Ghosh, H. N.; Ferrere, S.; Nozik A. J.; Lian, T. *J. Phys. Chem. B* **1999**, *103*, 3110−3119. (c) Ellingson, R. J.; Asbury, J. B.; Ferrere, S.; Ghosh, H. N.; Sprague, J. J.; Lian, T.; Nozik, A. *J. Phys. Chem. B* **1998**, *102*, 6455−6458.

(21) Hannappel, T.; Burfeindt, B.; Storck, W.; Willig, F. *J. Phys. Chem. B* **1997**, *101*, 6799−6802.

(22) Hannappel, T.; Zimmermann, C.; Meissner, B.; Burfeindt, B.; Storck, W.; Willig, F. *J. Phys. Chem. B* **1998**, *102*, 3651−3652.

(23) (a) Tachibana, Y.; Haque, S. A.; Mercer, I. P.; Durrant, J. R.; Klug, D. R. *J. Phys. Chem. B* **2000**, *104*, 1198−1205. (b) Tachibana, Y.; Moser, J. E.; Gratzel, M.; Klug, D. R.; Durrant, J. R. *J. Phys. Chem.* **1996**, *100*, 20056−20062.

(24) (a) Durrant, J. R.; Tachibana, Y.; Mercer, I. P.; Moser, J. E.; Gratzel, M.; Klug, D. R. *Z. Phys. Chem.* **1999**, *212*, 93. (b) Moser, J. E.; Noukakis, D.; Bach, U.; Tachibana, Y.; Klug, D. R.; Durrant, J. R.; Humphry-Baker, R.; Gratzel, M. *J. Phys. Chem. B* **1998**, *102*, 3649−3650.

(25) Heimer, T. A.; Heilweil, E. J.; Bignozzi, C. A.; Meyer, G. J. *J. Phys. Chem. A* **2000**, *104*, 4256−4262.

(26) Kallioinen, J.; Lehtovuori, V.; Myllyperkio, P.; Korppi-Tommola, J. *Chem. Phys. Lett.* **2001**, *340*, 217−221.

(27) (a) Nelson, J.; Haque, S. A.; Klug, D. R.; Durrant, J. R. *Phys. Rev. B.* **2001**, *63*, 205321−9. (b) Haque, S. A.; Tachibana, Y.; Willis, R. L.; Moser, J. E.; Gratzel, M.; Klug, D. R.; Durrant, J. R. *J. Phys. Chem. B* **2000**, *104*, 538−547. (c) Haque, S. A.; Tachibana, Y.; Klug, D. R.; Durrant, J. R. *J. Phys. Chem. B* **1998**, *102*, 1745−1749. (d) Pelet, S.; Moser, J. E.; Gratzel, M. *J. Phys. Chem. B* **2000**, *104*, 1791−1795.

(28) Kuciauskas, D.; Freund, M. S.; Gray, H. B.; Winkler, J. R.; Lewis, N. S. *J. Phys. Chem. B* **2001**, *105*, 392−403.

(29) (a) Kay, A.; Gratzel, M. *J. Phys. Chem.* **1993**, *97*, 6272−6277. (b) He, J.; Hagfeldt, A.; Lindquist, S.-E.; Grennberg, H.; Korodi, F.; Sun, L.; Akermark, B. *Langmuir* **2001**, *17*, 2743−2747. (c) Wang, Z.-S.; Li, F.-Y.; Huang, C.-H, Wang, L.; Wei, M.; Jin, L.-P.; Li, N.-Q. *J. Phys. Chem. B* **2000**, *104*, 9676−9682. (d) Islam, A.; Sugihara, H.; Yanagida, M.; Hara, K.; Fujihashi, G.; Tachibana, Y.; Katoh, R.; Murata, S.; Arakawa, H. *New J. Chem.* **2002**, *26*, 966−968. (e) Ren, Y.-J.; Tian, H.; Cai, S.-M. *New J. Chem.* **2002**, *26*, 184−187.

(30) Shoute, L. C. T.; Loppnow, G. R. *J. Chem. Phys.* **2002**, *117*, 842−850.

(31) (a) Lilichenko, M.; Tittlebach-Helmrich, D.; Verhoeven, J. W.; Gould, I. R.; Myers, A. B. *J. Chem. Phys.* **1998**, *109*, 10958−10968. (b) Kulinowski, K.; Gould, I. R.; Ferris, N. S.; Myers, A. B. *J. Phys. Chem.* **1995**, *99*, 17715−17723.

(32) (a) Blackbourn, R. L.; Johnson, C. S.; Hupp, J. T. *J. Am. Chem. Soc.* **1991**, *113*, 1060−1062. (b) Hupp, J. T.; Williams, R. D. *Acc. Chem. Res.* **2001**, *34*, 808−817. (c) Selmarten, D. C.; Hupp, J. T. *J. Chem. Soc., Faraday Trans.* **1996**, *92*, 3909−3916.

(33) (a) Huber, R.; Sporlein, S.; Moser, J. E.; Gratzel, M.; Wachtveitl, J. *J. Phys. Chem. B* **2000**, *104*, 8995−9003. (b) Kormann, C.; Bahnemann, D. W.; Hoffmann, M. R. *J. Phys. Chem.* **1988**, *92*, 5196−5201.

The experimental set up for measuring resonance Raman spectra and depolarization ratios has been described.[30,34] Laser excitation lines to cover the lowest-lying metal-to-ligand charge-transfer (MLCT) band of the N3|TiO_2 complex were obtained from an Ar ion (Coherent, Santa Clara, CA) laser (457.9, 488, and 514.5 nm) and a Kr ion (Coherent, Santa Clara, CA) laser (406.7, 530.9, 568.2, and 647 nm). For excitation wavelengths below 406.7 nm, laser lines from an Ar^+ pumped, mode-locked, picosecond Ti:sapphire (Coherent, Santa Clara, CA) oscillator operating in the spectral range of 700−900 nm were frequency doubled in a LBO nonlinear crystal to obtain the desired excitation wavelengths. The excitation laser beam was focused onto a spinning 5-mm o.d. NMR tube containing the sample. A known concentration of DMSO solvent served as the internal standard for the determination of the absolute Raman cross sections. The scattered Raman signals were collected in a 135° backscattering geometry and coupled into a spectrometer as described previously.[30,34] The dispersed Raman scattering in the visible range was detected with a multichannel liquid-nitrogen-cooled CCD (Princeton Instruments, Trenton, NJ) coupled to a single monochromator. The Raman scattering in the UV range was dispersed in a double monochromator and detected with a Pelletier-cooled UV-enhanced photodiode array (Princeton Instruments, Trenton, NJ). Measurements of the resonance Raman spectra and determinations of the intensities were repeated on 3−4 fresh samples. The sample spectra were frequency calibrated with known solvent Raman peaks and intensity corrected for the spectrometer detection efficiency by using a standard lamp (Electrooptics Associate). The concentration of N3 in the free N3 and in the N3|TiO_2 complex samples for resonance Raman measurements were determined from absorption spectroscopy by using a diode array spectrophotometer (Hewlett-Packard, model 8452A). Data analysis and the method that followed to determine absolute Raman cross sections from the experimentally measured resonance Raman intensities have been described previously.[30,34]

The absolute Raman cross sections of DMSO were determined against benzene as an internal standard.[35,36] The Raman spectra of 2 M benzene in DMSO were measured for laser excitation wavelengths at 406.7, 457.9, 488, 514.5, 530.9, 568.2, and 647 nm. Raman cross sections for DMSO at each excitation wavelength were then calculated from the integrated areas under each DMSO line from the benzene Raman line at 992 cm^{-1} as reference using the following equation:[30,34]

$$\sigma_S = \sigma_R \frac{I_S}{I_R}\frac{[R]}{[S]}\frac{E_R}{E_S}\frac{L_R}{L_S}\frac{n_S}{n_R}\left(\frac{1+\rho_R}{1+2\rho_R}\frac{1+2\rho_S}{1+\rho_S}\right)10^{dc(\epsilon_S-\epsilon_R)} \quad (1)$$

where σ, I, E, L, n, and ρ are the absolute cross section, integrated Raman scattering intensity, spectrometer efficiency, internal field correction $\{L = [(n^2 + 2)/3]^4\}$, refractive index, and depolarization ratio, respectively. The subscripts R and S refer to reference and sample, which are present in solution with concentration [R] and [S]. The self-absorption term[34] has $d = -\log 0.5/c\epsilon_l$; c is the concentration of the absorbing species, and ϵ is the extinction coefficients of the absorber at the frequencies of laser excitation (ϵ_l), Raman scattering for the sample (ϵ_S), and Raman scattering for the reference (ϵ_R). An A-term equation (eq 2)[37] was fit to the resulting DMSO Raman cross sections obtained for the 668-cm^{-1} band of DMSO

$$\sigma_R = \frac{8\pi}{3}\left(\frac{1+2\rho}{1+\rho}\right)K\bar{\nu}_0\bar{\nu}^3\left[\frac{\bar{\nu}_e^2+\bar{\nu}_0^2}{(\bar{\nu}_e^2-\bar{\nu}_0)^2}+C\right]^2 \quad (2)$$

to yield $K = 9.57 \times 10^{-30}$ cm^2/molecule, $\rho = 0.06$, $\bar{\nu}_e = 51\,940$ cm^{-1}, and $C = 3.32 \times 10^{-9}$ cm^2, where, $\bar{\nu}_e$ is the resonant electronic energy, $\bar{\nu}_0$ and $\bar{\nu}$ are the incident and scattered photon energies, ρ is the depolarization ratio, K is a constant, and C is the contribution from background electronic states. Equation 2 with these parameters was then used to calculate the absolute Raman cross sections of DMSO at each excitation wavelength. Similar A-term parameters were obtained when the absolute Raman cross sections of DMSO solvent were determined against neat benzene as an external standard. The experimental absolute Raman cross sections of the 2911-cm^{-1} band of neat DMSO were determined from the sum of the absolute Raman cross sections of cyclohexane Raman bands[35] in the region 2853−2938 cm^{-1} as external standard by the procedure described above. These cross-sections were then fit to eq 2 using $K = 7.44 \times 10^{-29}$ cm^2/molecule, $\bar{\nu}_e = 51\,940$ cm^{-1}, and $C = 6.25 \times 10^{-10}$ cm^2. The cross sections used at each laser excitation wavelength were calculated from eq 2 using these parameters.

Theory

The absorption spectrum and resonance Raman cross sections were calculated using the time-dependent wave packet formalism first introduced by Heller and co-workers:[38,39] In the analysis presented here, two close-lying electronic transitions are considered to contribute to the resonance Raman intensities. When two or more electronic transitions overlap or nearly overlap, the Raman intensities obtained in the region spanning these transitions are influenced by both the interference and pre-resonance terms, and the shape of the profiles depends on the relative transition dipole moments and the mode displacements. The Raman cross section, $\sigma_{i\to f}$, at the excitation laser frequency ω_L within the Condon approximation is given by[31a,40]

$$\sigma_{I\to F}(\omega_L,\delta) = \frac{8\pi e^4 {\omega_S}^3 \omega_L}{9c^4}\sum_i B_i \int_{-\infty}^{\infty} d\delta\, H(\delta)|\alpha_{i\to f}^{tot}|^2 \quad (3)$$

where, ω_L and ω_S are frequencies of the incident laser and scattered Raman, B_i is the Boltzmann population of the initial state, $\delta = \hbar(\varpi_0 - \omega_0)$ is the shift from the central zero−zero frequency, ϖ_0, due to inhomogeneous broadening, and $H(\delta) = (1/\theta(2\pi)^{1/2})\exp[-\delta^2/2\theta^2]$ is a normalized Gaussian distribution of site electronic energies. In this expression, α_k^{tot} is the sum of the Raman polarizabilities of the electronic transitions considered in the calculation. For two electronic transitions, the polarizability becomes

$$\alpha_{i\to f}^{tot} = \alpha_1 + \alpha_2 \quad (4)$$

$$\alpha_k(\omega_L,\delta) = \frac{2\pi|\mu_{k0}|^2}{\hbar}\int_0^{\infty} dt\langle\chi_f|\chi_i^k(t)\rangle\exp[i(\omega_L - \omega_k - \delta + \omega_i)t]G(t) \quad (5)$$

where μ_{k0} is the coordinate independent transition dipole moment of electronic state k, ω_k is the electronic zero−zero transition frequency to state k, $h\omega_i/2\pi$ is the energy of the initial vibrational level of the ground electronic state, $|\chi_i\rangle$ and $|\chi_f\rangle$ are

(34) Fraga, E.; Webb, M. A.; Loppnow, G. R. *J. Phys. Chem.* **1996**, *100*, 3278−3287.
(35) Trulson, M. O.; Mathies, R. A. *J. Chem. Phys.* **1986**, *84*, 2068−2074.
(36) Schomacker, K. T.; Delaney, J. K.; Champion, P. M. *J. Chem. Phys.* **1986**, *85*, 4240−4247.
(37) Albrecht, A. C.; Hutley, M. C. *J. Chem. Phys.* **1971**, *55*, 4438−4443.
(38) (a) Lee, S. Y.; Heller, E. J. *J. Chem. Phys.* **1979**, *71*, 4777−4788. (b) Tannor, D. J.; Heller, E. J. *J. Chem. Phys.* **1982**, *77*, 202−218.
(39) (a) Myers, A. B.; Mathies, R. A. Resonance Raman Intensities: A Probe of Excited-State Structure and Dynamics. In *Biological Applications of Raman Spectroscopy*; Spiro, T. G., Ed.; Wiley: New York, 1987; Vol. 2, p 1. (b) Myers, A. B. Excited Electronic State Properties from Ground-state Resonance Raman Intensities. In *Laser Techniques in Chemistry*; Myers, A. B., Rizzo, T. R., Eds. Wiley: New York, 1995; p 325. (c) Kelley, A. M. *J. Phys. Chem. A* **1999**, *103*, 6891−6903.
(40) Egolf, D. S.; Waterland, M. R.; Kelley, A. M. *J. Phys. Chem. B* **2000**, *104*, 10727−10737.

the initial and final vibrational wave functions, respectively, and $|\chi_i^k(t)\rangle = \exp(iH_k t/\hbar)|\chi_i\rangle$ is the initial vibrational wave function propagated for time t by the excited-state vibrational Hamiltonian H_k. At the same level of theory, the absorption cross section at frequency ω_L is given by

$$\sigma_A(\omega_L) = \sum_{k=1,2} \frac{4\pi|\mu_{k0}|^2\omega_L}{3n\hbar c} \sum_i B_i \int_{-\infty}^{\infty} d\delta H(\delta) \int_{-\infty}^{\infty} dt \langle\chi_i|\chi_i^k(t)\rangle \exp[i(\omega_L - \omega_k - \delta + \omega_i)t] G(t) \quad (6)$$

In both of these expressions, the damping function, $G(t) = \exp[-g_{solv}(t)]$ is the homogeneous broadening function due to solvent-induced pure dephasing. For molecules interacting with a bath, $G(t)$ represents the dynamics of chromophore-solvent coupling. The Brownian oscillator model developed by Mukamel and co-workers[41,42] is adopted to model the solute−solvent interactions that contribute to the solvent-induced homogeneous broadening. This model treats the solvent response as arising from one or more linearly coupled vibrational modes each characterized by a frequency, a ground-to-excited state displacement, and an arbitrary frictional damping. For simplicity, all the solvent degrees of freedom are treated as one effective mode. When the friction on this mode is high or the oscillator is strongly overdamped, the dephasing function $g_{solv}(t)$ has both real and imaginary parts:

$$g_{solv}(t) = g_R(t) + ig_I(t) \quad (7)$$

In the high-temperature limit ($\hbar/\Lambda << kT$),

$$g_R(t) = \frac{D^2}{\Lambda^2}[\exp(-\Lambda t/\hbar) - 1 + \Lambda t/\hbar] \quad (8)$$

$$g_I(t) = \frac{D^2}{2kT\Lambda}[1 - \exp(-\Lambda t/\hbar)] \quad (9)$$

Where D represents the strength of the coupling between the electronic transition and the solvent coordinate, T is the temperature, and $\hbar/\Lambda$ gives the characteristic solvent time scale. The imaginary component of $g_{solv}(t)$ accounts for the solvation. As the solvent time scale becomes long ($\kappa = \Lambda/D \rightarrow 0$), it assumes the form

$$g_I(t) = \frac{D^2 t}{2kT\hbar} = \frac{\lambda_S t}{\hbar} \quad (10)$$

where λ_S is the solvent contribution to the reorganization energy. The implementation of these equations to the resonance Raman intensities of charge-transfer systems has been described in detail.[30,31,34,39−42]

For the analysis presented here, the initial guesses for the displacements along each normal coordinate (Δ) were found from the relative resonance Raman vibrational intensities at 514.5 nm, assuming the intensities were proportional to Δ^2 and with the Δ of the 1544 cm^{-1} mode set initially to 1. All of the observed fundamental vibrational modes were used in the time-dependent calculations. Other parameters were selected to give the best calculated absorption spectrum and resonance Raman excitation profiles. The parameters were then optimized iteratively as described previously[30,34] until the calculated and experimental absorption spectra and resonance Raman excitation profiles were in agreement.

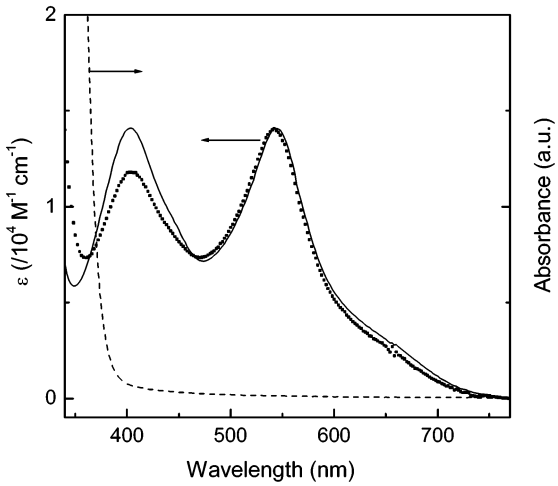

Figure 1. Absorption spectra of aqueous TiO_2 nanoparticles (- - -) and of N3 (—) and N3|TiO_2 (·····) in DMSO. The extinction coefficient of the TiO_2 nanoparticles was not determined quantitatively, so its spectrum is shown for illustration only.

Results

Figure 1 presents the absorption spectra of free N3 and N3|TiO_2 in DMSO. The spectrum of N3 has intense absorption bands at 402 and 544 nm attributed to allowed singlet metal-to-ligand charge-transfer (^{1}MLCT) transitions and a long wavelength tail extending to the red attributed to the spin-forbidden triplet metal-to-ligand charge-transfer (^{3}MLCT) transition. The lowest-energy ^{1}MLCT and ^{3}MLCT bands of N3|TiO_2 have similar band shapes as in the free N3, and the ^{1}MLCT band is very slightly blue-shifted (544 nm to 542 nm). The spectrum of the N3|TiO_2 complex below 380 nm exhibits strong absorption due to TiO_2 nanoparticles as shown in Figure 1. Determination of the absorption coefficient of the N3|TiO_2 complex from an optical density versus concentration plot gives a value of $(1.41 \pm 0.3) \times 10^4$ M^{-1} cm^{-1}, identical to that of the free N3 reported in the literature.[4] These results indicate that there is only weak electronic interaction between TiO_2 and the adsorbed N3, consistent with the small electronic coupling of 130 cm^{-1} reported for this complex.[43] The free N3 in aqueous solution emits luminescence[4] at 750 nm (not shown), which is quenched upon binding to TiO_2. The luminescence quenching and increase in the solubility of N3 with the N3|TiO_2 complex formation provide evidence for the adsorption of N3 onto the surface of TiO_2. From the luminescence signal-to-noise ratio, we estimate that ≤5% of the dye exists as free dye in the N3|TiO_2 sample. Because the resonance Raman cross sections for the free dye are smaller by a factor of 1.5−2, the free dye contributes only ∼3% of the observed resonance Raman scattering from N3|TiO_2.

Figures 2 and 3 present the resonance Raman spectra of free N3 and the N3|TiO_2 complex in DMSO. The spectra are similar

(41) Mukamel, S. *Principles of nonlinear optical spectroscopy*; Oxford University Press: New York, 1995.
(42) Li, B.; Johnson, A. E.; Mukamel, S.; Myers, A. B. *J. Am. Chem. Soc.* **1994**, *116*, 11039−11047.
(43) Moser, J. E.; Bonnote, P.; Gratzel, M. *Coord. Chem. Rev.* **1998**, *171*, 245−250.

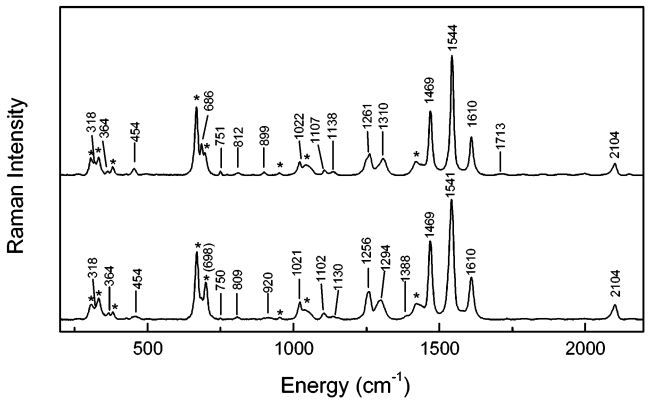

Figure 2. Resonance Raman spectra obtained with excitation at 514.5 nm of 4 mM N3 (top) and N3|TiO_2 (bottom) containing 4 mM N3 in DMSO. The top spectrum has been displaced vertically for clarity. Asterisks (*) indicate bands due to DMSO.

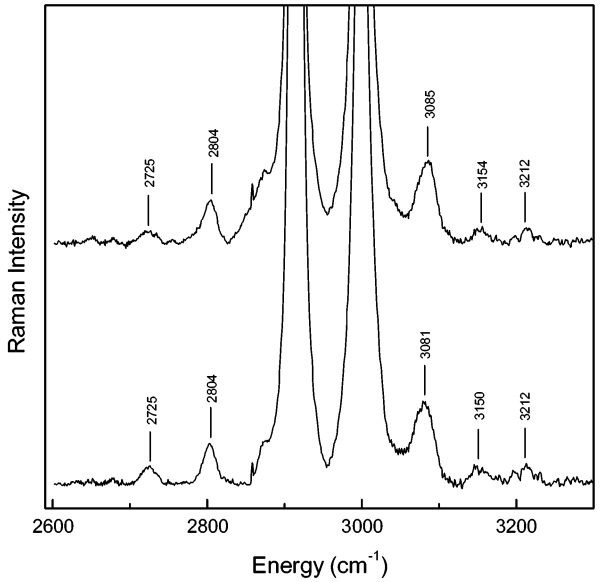

Figure 3. Resonance Raman spectra in the overtone region obtained with excitation at 514.5 nm of 4 mM N3 (top) and N3|TiO_2 (bottom) containing 4 mM N3 in DMSO. The top spectrum has been displaced vertically for clarity. The two strong bands at ~2900 and ~3000 cm^{-1} arise from the DMSO solvent. The spectra have been expanded along the *Y*-axis to more clearly show the solute bands.

to those reported in the literature.[44] The Raman bands in the 300−2200 cm^{-1} region of Figure 2 have been assigned to fundamental vibrations. The peak positions of the Raman lines and their assignments[44−47] are listed in Tables 1 and 2. The resonance Raman spectrum of the N3|TiO_2 complex in DMSO solution is similar to that of free N3 in DMSO, indicating that complexation with TiO_2 has little affect on the resonance-enhanced vibrational frequencies or modes of the adsorbed N3 molecule. The intense bipyridine ring-stretching mode at 1544 cm^{-1} of free N3 is downshifted by only 3 cm^{-1} in the complex N3|TiO_2, while the two other relatively intense bipyridine ring-stretching modes at 1610 and 1469 cm^{-1} and the ring breathing mode at 1022 cm^{-1} are unaffected by complexation. Large downshifts are observed for the C—C inter-ring and C—O

Table 1. Spectral Modeling Parameters for the Free N3 in DMSO

		^{3}MLCT		^{1}MLCT		
$\tilde{\nu}$/cm^{-1}	ρ^a	$\lvert\Delta\rvert^b$	λ_v/cm^{-1}	$\lvert\Delta\rvert^b$	λ_v/cm^{-1c}	assignments[d]
318		0.08	1.02	0.08	1.02	Ru—N stretch
364		0.06	0.66	0.06	0.66	Ru—N stretch
454		0.09	1.84	0.09	1.84	out-of-plane ring deformation
686	0.31	0.10	3.43	0.104	3.71	in-plane ring deformation
751	0.37	0.038	0.54	0.037	0.52	in-plane ring deformation
812	0.24	0.037	0.56	0.037	0.54	C═S stretch, out-of-plane ring def.
899	0.30	0.037	0.62	0.036	0.60	out-of-plane C—H deformation
1022	0.34	0.10	5.11	0.097	4.84	bpy ring breathing
1107	0.23	0.038	0.80	0.037	0.76	in-plane C—H wagging
1138	0.33	0.37	0.78	0.036	0.72	in-plane C—H wagging
1261	0.33	0.13	10.66	0.120	9.08	C—C inter-ring, C—O stretch
1310	0.30	0.097	6.16	0.096	5.99	C—C inter-ring, C—O stretch
1469	0.34	0.17	21.23	0.164	19.87	bpy ring stretch
1544	0.33	0.22	37.37	0.209	33.77	bpy ring stretch
1610	0.44	0.13	13.6	0.124	12.29	bpy ring stretch
1713	0.23	0.032	0.88	0.032	0.88	C═O stretch
2104		0.08	6.73	0.078	6.33	C═N stretch
3085						2 × 1544
3154						1544 + 1610
3212						2 × 1610
total vibrational reorganization energy = 215.4 cm^{-1}						

[a] The depolarization ratio, ρ, is the ratio of the Raman scattering intensities having polarizations perpendicular and parallel to that of the laser. [b] The displacement parameters, Δ, were obtained by fitting eqs 3 and 6 assuming overlapping ^{1}MLCT and ^{3}MLCT electronic transitions with the following parameters: electronic zero−zero energy E_{00} = 17 815 cm^{-1} and transition length μ = 1.08 Å in ^{1}MLCT; E_{00}= 15 100 cm^{-1} and μ = 0.55 Å in ^{3}MLCT, homogeneous broadening Γ = 1055 cm^{-1}, inhomogeneous broadening (standard deviation) Θ = 870 cm^{-1}, line shape parameter for Brownian oscillator $\kappa = \Lambda/D = 0.1$. Typical errors on the Δ's are ±20%. [c] The vibrational reorganization energy $\lambda_v = \Delta^2\bar{\nu}/2$. [d] The vibrational mode assignments are from refs 44−47.

Table 2. Spectral Modeling Parameters for the N3|TiO_2 Complex in DMSO

		^{3}MLCT		^{1}MLCT		
$\tilde{\nu}$/cm^{-1}	ρ^a	$\lvert\Delta\rvert^b$	λ_v/cm^{-1}	$\lvert\Delta\rvert^b$	λ_v/cm^{-1c}	assignments[d]
318		0.006	0.006	0.006	0.006	Ru—N stretch
364		0.037	0.25	0.037	0.25	Ru—N stretch
454		0.03	0.20	0.03	0.20	out-of-plane ring deformation
698	0.31	0.080	2.23	0.080	2.23	in-plane ring deformation
750	0.37	0.020	0.15	0.020	0.15	in-plane ring deformation
809	0.24	0.033	0.44	0.033	0.44	C═S stretch, out-of-plane ring def.
920	0.30	0.029	0.39	0.029	0.39	out-of-plane C—H deformation
1021	0.34	0.061	1.90	0.061	1.90	bpy ring breathing
1102	0.23	0.028	0.43	0.028	0.43	in-plane C—H wagging
1130	0.33	0.026	0.38	0.026	0.38	in-plane C—H wagging
1256	0.33	0.089	4.97	0.089	4.97	C—C inter-ring, C—O stretch
1294	0.30	0.071	3.26	0.071	3.26	C—C inter-ring, C—O stretch
1388		0.022	0.34	0.022	0.34	symmetric stretch —CO_2^-
1469	0.34	0.118	10.23	0.118	10.23	bpy ring stretch
1541	0.33	0.159	19.48	0.159	19.48	bpy ring stretch
1610	0.44	0.094	7.14	0.094	7.14	bpy ring stretch
2104		0.060	3.79	0.060	3.79	C═N stretch
3081						2 × 1541
3150						1541 + 1610
3212						2 × 1610
total vibrational reorganization energy = 112.0 cm^{-1}						

[a] Same as in Table 1. [b] The displacement parameters, Δ, were obtained by fitting eqs 3 and 6 assuming overlapping ^{1}MLCT and ^{3}MLCT electronic transitions with the following parameters: electronic zero−zero energy E_{00} = 18 330 cm^{-1} and transition length μ = 1.055 Å in ^{1}MLCT; E_{00}= 15 750 cm^{-1} and μ = 0.53 Å in ^{3}MLCT, homogeneous broadening Γ = 422 cm^{-1}, inhomogeneous broadening (standard deviation) Θ = 960 cm^{-1}, line shape parameter for Brownian oscillator $\kappa = \Lambda/D = 0.1$. Typical errors on the Δ's are ±20%. [c] Same as in Table 1. [d] Same as in Table 1.

(44) (a) Greijer, H.; Lindgren, J.; Hagfeldt, A. *J. Phys. Chem. B* **2001**, *105*, 6314−6320. (b) Goff, A. H.-L.; Joiret, S.; Falaras, P. *J. Phys. Chem. B* **1999**, *103*, 9569−9575. (c) Zakeeruddin, S. M.; Nazeeruddin, M. K.; Pechy, P.; Rotzinger, F. P.; Humphry-Baker, R.; Kalyanasundaram, K.; Gratzel, M.; Shklover, V.; Haiback, T. *Inorg. Chem.* **1997**, *36*, 5937−5946.
(45) (a) Strommen, D. P.; Mallick, P. K.; Danzer, G. D.; Lumpkin, R. S.; Kincaid, J. R. *J. Phys. Chem.* **1990**, *94*, 1357−1366. (b) Mallick, P. K.; Danzer, G. D.; Strommen, D. P.; Kincaid, J. R. *J. Phys. Chem.* **1988**, *92*, 5628−5634.
(46) Maillick, P. K.; Danzer, G. D.; Strommen, D. P.; Kincaid, J. R. *J. Am. Chem. Soc*. **1990**, *112*, 1686−1690.
(47) Umapathy, S.; Lee-Son, G.; Hester, R. E. *J. Mol. Struct.* **1989**, *194*, 107−116.

stretching modes at 1261 and 1310 cm^{-1}, as the N3 dye is bound to TiO_2 via the carboxylate groups on the ligands. Relatively large downshifts are also observed for the C—H in-plane wagging modes at 1107 and 1138 cm^{-1}. The C═S and C═N stretching modes at 812 and 2104 cm^{-1} due to thiocyanate ligands are relatively unaffected in the N3|TiO_2 complex, as this ligand does not participate in the binding. The C═O stretching band at 1713 cm^{-1} appears as a very weak band in the free N3 but is absent in the N3|TiO_2 complex. A weak out-of-plane C—H deformation band at 899 cm^{-1} in N3 is shifted to 920 cm^{-1} in N3|TiO_2. The most intense band in the low-frequency region is the 686 cm^{-1} in-plane ring deformation mode, which shifts to 698 cm^{-1} and appears more intense in N3|TiO_2, indicating that this mode is strongly affected by binding to the surface of TiO_2. This band overlaps with the solvent 699 cm^{-1} but is evidenced by an increase in the intensity of this band relative to the solvent 668 cm^{-1} band as the excitation wavelength is tuned to the N3 absorption maximum. In N3|TiO_2, a weak band attributed to the symmetric $-CO_2^-$ stretching mode[48,49] appears at 1388 cm^{-1} but is absent in N3. To determine that this band is not due to the overtone of the strong 698 cm^{-1} band of N3|TiO_2, we have calculated the overtone intensity using eq 3 and the parameters of Table 2. The calculated overtone Raman cross section of the 698 cm^{-1} mode of 2.5×10^{-11} $Å^2$ $molecule^{-1}$ is an order of magnitude less than the observed cross section for the 1388 cm^{-1} mode (3.6×10^{-10} $Å^2$ $molecule^{-1}$), indicating that it is a fundamental mode. In agreement with our previous work on Alz|TiO_2, we observed no bands attributable to modes originating from TiO_2.

A number of Raman lines in the high-frequency region have been assigned to overtone and combination bands and are shown in Figure 3. In N3, the most intense line at 3085 cm^{-1} is the overtone of the 1544 cm^{-1} mode, and the relatively weak bands at 3154 and 3212 cm^{-1} are combination (1544 + 1610 cm^1) and overtone (2 × 1610 cm^1) bands, respectively. The corresponding bands for N3|TiO_2 are at 3081, 3150, and 3212 cm^{-1}. A couple of very weak fundamental CH stretching modes are observed at 2725 and 2804 cm^{-1} for both N3 and N3|TiO_2. The intensities of these bands are an order of magnitude weaker than the fundamentals of the fingerprint region and, hence, were not included in the simulation. The depolarization ratios measured on excitation at 530.9 nm (Table 1) for all the observed Raman lines are close to 0.33 within experimental error, the value expected for modes resonantly enhanced by a single electronic transition. The depolarization ratios measured at the 457.9 nm excitation, where there is considerable overlap with the higher ^{1}MLCT electronic state, gave values similar to those at the 530.9 nm excitation, indicating that these two electronic states have parallel transition dipole moments or that the resonance enhancement is significantly stronger with the 544-nm electronic transition.

Figure 4 shows the experimental and calculated absorption spectra of N3 and N3|TiO_2 in DMSO using eq 6 and the parameters of Tables 1 and 2. For the absorption spectrum, two models were used, one assuming a contribution from only a single ^{1}MLCT transition and another assuming two resonant states, a singlet ^{1}MLCT and a nearby triplet ^{3}MLCT state. The calculated absorption spectrum assuming a single resonant electronic state (dotted line in Figure 4) completely fails to account for the long wavelength tail of the experimental absorption spectrum. Clearly, the two-electronic-state model (dashed line in Figure 4) is more accurate. The lowest-energy ^{1}MLCT electronic state of N3 has two nearby excited electronic states which can interfere with the electronic transition. The first is a spin-forbidden, weak ^{3}MLCT ($S_0 \rightarrow T_1$) transition, which appears as a shoulder in the long wavelength tail of the spectrum. For N3, the simulations show that this band has $E_{00} = 15\,100$ cm^{-1} and a transition moment of 0.55 Å and is merely 2700 cm^{-1} from the strong, lowest-energy ^{1}MLCT ($E_{00} = 17\,815$ cm^{-1} and $\mu = 1.08$ Å) transition. The second is a higher-lying, spin-allowed ^{1}MLCT transition, which has a similar transition dipole moment as the resonant state and appears much further, 6400 cm^{-1}, to the blue of the resonant state. This state may also exert an interference effect on the resonance Raman spectrum excited within the first ^{1}MLCT state but was not included in the simulations (vide infra).

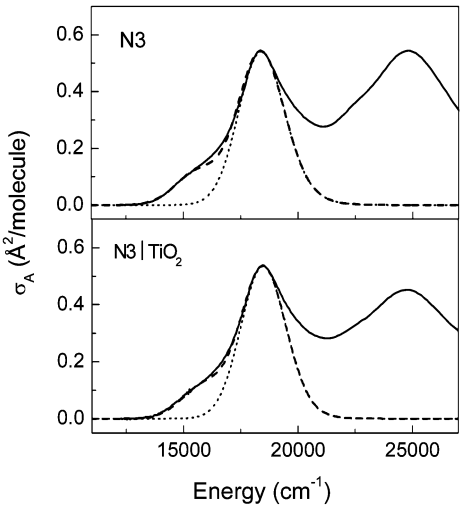

Figure 4. Experimental (—) and calculated (– –) absorption spectra assuming contributions from two electronic states for N3 (top) and N3|TiO_2 (bottom) in DMSO using eq 6 and the parameters in Tables 1 and 2, respectively. The dotted line (·····) is the calculated absorption spectrum assuming a single electronic transition for N3 (top) and N3|TiO_2 (bottom).

Figures 5 and 6 show the experimental and calculated resonance Raman excitation profiles for N3 and N3|TiO_2, respectively, using eq 3 and the parameters of Tables 1 and 2. The best fit to the profiles was obtained by simultaneously fitting all the observed resonance-enhanced fundamental modes and the absorption spectrum, which was assumed to have contributions from two electronic transitions, the ^{1}MLCT at 544 nm and the ^{3}MLCT at 625 nm. The calculated absorption spectrum and the resonance Raman excitation profiles are in good agreement with the experimental values. Since Raman intensity is proportional to the fourth power of the transition dipole moment, the contribution of the lowest-lying ^{1}MLCT will dominate in the region where the absorption of both of the ^{1}MLCT and ^{3}MLCT states significantly overlap. The resonance Raman excitation profiles obtained on excitation at a wavelength region where the first and second ^{1}MLCT bands overlap show no significant interference effects, although the latter state

(48) (a) Murakoshi, K.; Kano, G.; Wada, Y.; Yanagida, S.; Miyazaki, H.; Matsumoto, M.; Murasawa, S. *J. Electroanal. Chem.* **1995**, *396*, 27−34. (b) Meyer, T.; Meyer, G. J.; Pfennig, B. W.; Schoonoover, J. R.; Timpson, C. J.; Wall, J. F.; Kobusch, C.; Xiaohong, C.; Peek, B. M.; Wall, C. G.; Ou, W.; Erickson, B. W.; Bignozzi, C. A. *Inorg. Chem.* **1994**, *33*, 3952−3964. (c) Fillinger, A.; Parkinson, B. A. *J. Electrochem. Soc.* **1999**, *146*, 4559−4564.
(49) Finnie, K.; Bartlett, J. R.; Woolfrey, J. L. *Langmuir* **1998**, *14*, 2744−2749.

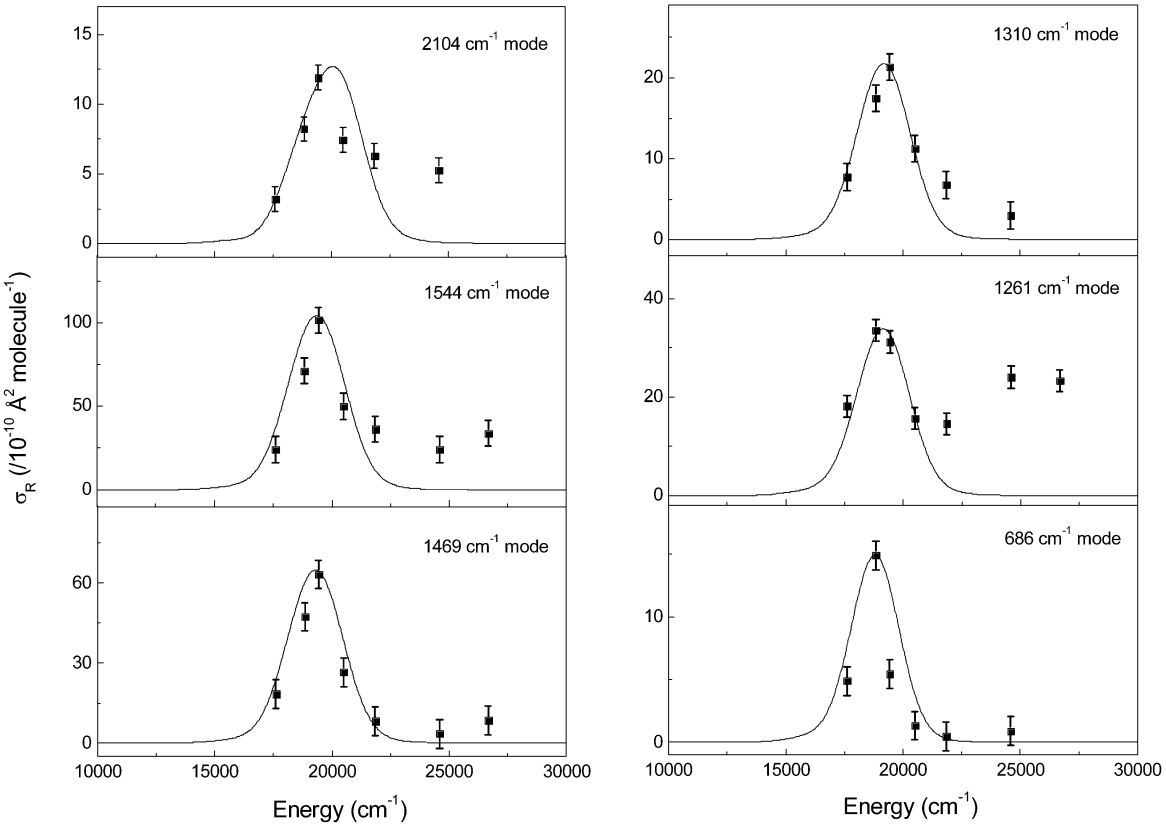

Figure 5. Experimental (■) and calculated (—) resonance Raman excitation profiles of the six most intense modes of N3 in DMSO. Calculations used eq 3 and the parameters of Table 1. Deviations between the calculated and experimental cross sections at energies >22 500 cm^{-1} are due to resonance enhancement by the ~400-nm, higher-lying ^{1}MLCT state, which was not modeled here.

weakly enhances the vibrational modes of a few modes, such as the 1262, 1544, and 2104 cm^{-1} modes (Figures 5 and 6).

An interesting result is that the set of excited-state displacements (i.e., the differences between the ground and excited state along each normal mode = Δ) are significantly smaller for the N3|TiO_2 complex than for the free N3 (compare Tables 1 and 2), by 25−30%. This result is significant, as it indicates that the TiO_2 nanoparticle has an affect on the intramolecular electron-transfer dynamics of the adsorbed dye. Modeling the experimental data with eqs 3 and 6 has indicated that a range of Δ values could be used to fit the absorption spectrum and the fundamental resonance Raman excitation profiles equally well. It is well-known that the overtone and combination band intensities are much more sensitive to the Δ values and provide a more sensitive constraint on the excited-state parameters. Figure 7 shows how a small change in the scaling of the Δ values significantly affects the fit to the overtone profiles even when the absorption spectra and fundamental resonance Raman excitation profiles are reproduced well. All sets of parameters used to fit the overtone profiles in Figure 7 fit the absorption spectra and the fundamental resonance Raman excitation profiles equally well. Tables 1 and 2 list the parameters for N3 and N3|TiO_2, which best reproduce all the absorption and Raman experimental data.

A fundamental question that needs to be addressed is whether the effect of TiO_2 on the excited-state dynamics of the adsorbed N3 is due to an intrinsic or ensemble property of the system. Since the effect on the excited-state dynamics is reflected in the absolute resonance Raman cross section of each mode, we have measured the absolute resonance Raman cross sections of the fundamental modes of N3|TiO_2 as a function of the number of N3 dye molecules adsorbed per TiO_2 nanoparticle. Figure 8 shows the effect of changing N3 concentration, at constant TiO_2 concentration, on the absolute resonance Raman cross section of the most intense 1541 cm^{-1} mode of N3|TiO_2 in DMSO. Extrapolation to an N3 concentration of ~0 corresponds to a single N3 dye molecule bound to a TiO_2 nanoparticle (or 1:1 complex), and a 4 mM N3 concentration corresponds to ca. 500 N3 molecules adsorbed on a single TiO_2 nanoparticle (or a monolayer coverage). The <12% change in the absolute resonance Raman cross sections observed in this range is within the expected experimental error in our measurements. Similar variation in the absolute resonance Raman cross sections of the fundamental modes is observed for the free N3 as shown in Figure 8 for the most intense 1544 cm^{-1} mode. These results clearly indicate that the effect of TiO_2 on the excited-state dynamics of the adsorbed N3 is due to the intrinsic binding between TiO_2 and N3.

Discussion

In a recent resonance Raman study of alizarin-sensitized TiO_2 nanoparticles[30] (Alz|TiO_2), we observed an anomalously small reorganization energy for the charge injection, indicating that the TiO_2 nanoparticle appears to have a strong effect on charge-transfer dynamics. Further, all the internal reorganization energy originates from the donor alizarin modes, with no contributions from the accepting TiO_2 nanoparticle modes. This is in contrast to normal homogeneous charge transfer where the internal reorganization energy contains contribution from the vibrational modes of both the donor and acceptor molecules.[31] Since the

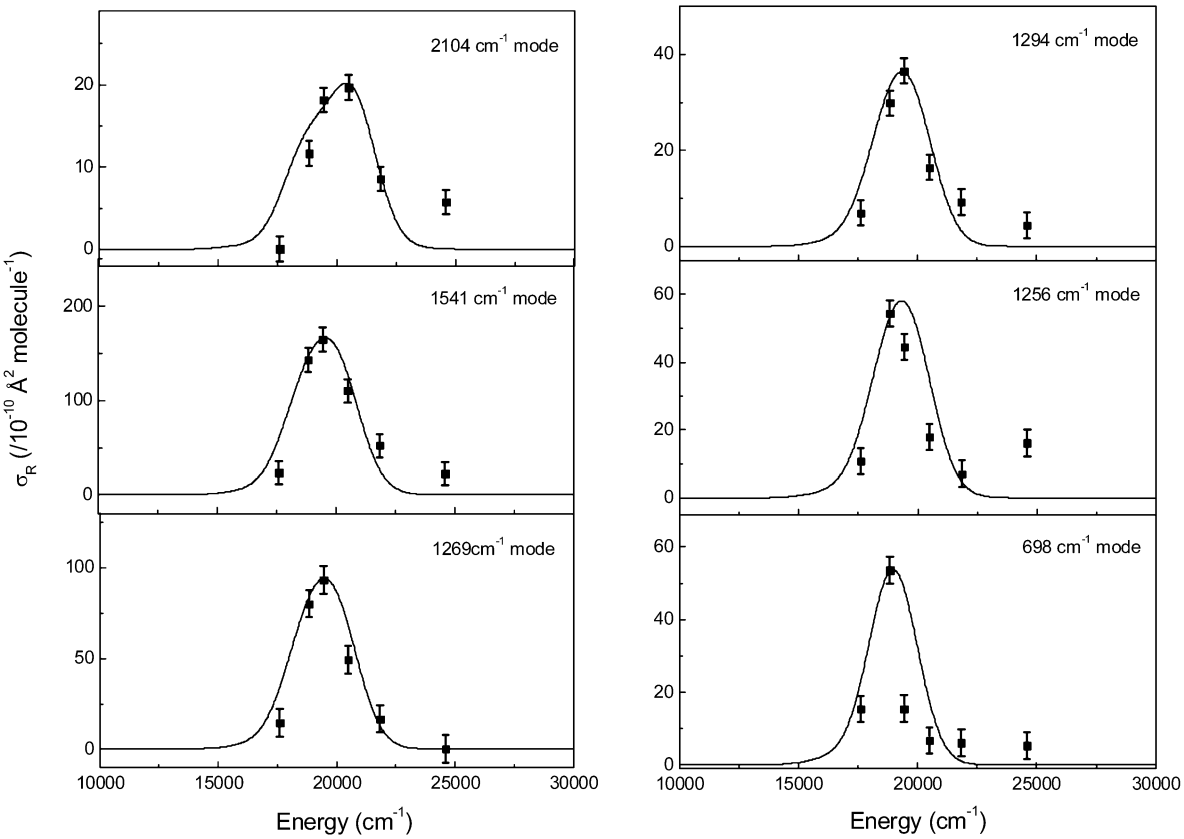

Figure 6. Same as in Figure 5 but for N3|TiO_2 in DMSO.

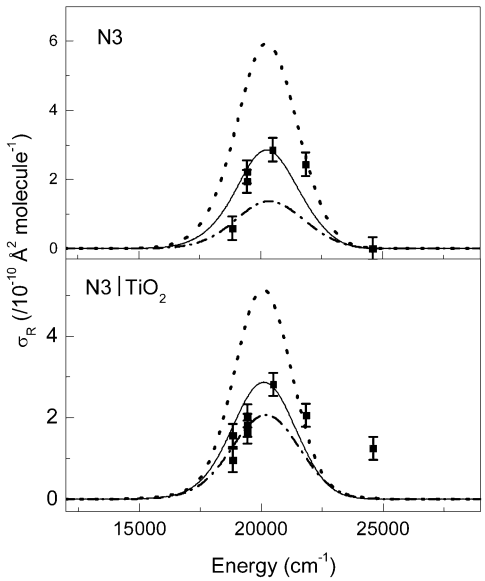

Figure 7. Experimental (■) and calculated (—) resonance Raman excitation profiles of the 3085 cm^{-1} overtone band of N3 (top) and 3081 cm^{-1} overtone band of N3|TiO_2 (bottom) in DMSO using eq 3 and the parameters of Tables 1 and 2, respectively. The dotted line (·····) and dashed dot line (− • −) represent the calculated overtone excitation profiles with 1.5 times (Γ = 840 cm^{-1}, Θ = 880 cm^{-1}) and 0.8 times (Γ = 260 cm^{-1}, Θ = 1120 cm^{-1}) the Δ's listed in Tables 1 and 2, respectively. The other parameters were adjusted to give a comparable fit to the absorption and fundamental resonance Raman excitation profiles as in Figures 4−6.

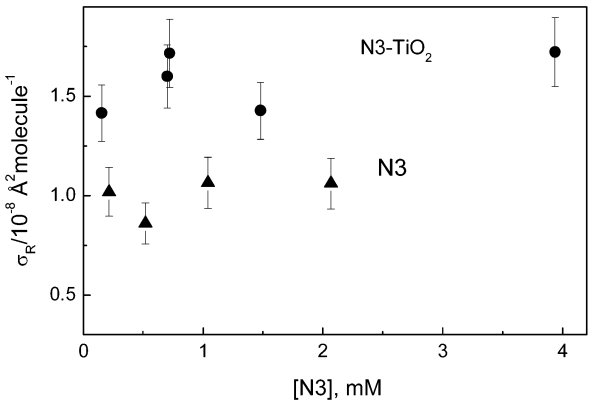

Figure 8. Dependence of the absolute resonance Raman cross section on N3 concentration in DMSO for N3|TiO_2 (●) and free N3 (▲) at constant TiO_2 concentration.

accepting conduction band of the TiO_2 nanoparticle has a high density of electronic states and the surface TiO_2 units, which are bound to alizarin, are strongly coupled to the interior of the nanoparticle, it was assumed that rapid electronic and/or vibrational dephasing could damp out the TiO_2 modes. These effects have been proposed as the reason for the observed small reorganization energy for Alz|TiO_2. However, a more definitive conclusion on the effects of the TiO_2 nanoparticle on the excited-state charge-transfer dynamics could not be made in the absence of data on the uncomplexed alizarin dye due to fluorescence.

In this paper, the key question being explored is what is the effect of the TiO_2 surface and adsorption upon the intramolecular MLCT excited-state dynamics. By comparing the resonance Raman-derived excited-state parameters of N3 and N3|TiO_2, the effects of the TiO_2 surface can be unambiguously measured.

Complex Formation and Bonding. The ligand of the N3 dye has four carboxylic acid groups, which form bonds to the surface groups on TiO_2 nanoparticles. Each carboxylic acid

group could potentially form an ester bond with the surface TiOH group leading to a unidentate linkage.[48,49] Each could also chelate with a single Ti^{4+} ion or two Ti^{4+} ions leading to a bidentate or a bridging bond, respectively. Recently, Finnie et al.[49] used the splitting of asymmetric and symmetric carboxylate stretching bands in the IR spectrum to distinguish the possible modes of coordination of N3 to the surface of TiO_2 nanoparticles. Based on the similar splitting observed in the IR bands of the asymmetric (1610 cm^{-1}) and symmetric (1380 cm^{-1}) carboxylate stretching vibrations of the adsorbed N3 and fully ionized N3, they concluded that N3 forms either a bidentate or bridging bond with TiO_2 nanoparticles. In our resonance Raman spectrum of N3|TiO_2, we observed the symmetric carboxylate stretching band at 1388 cm^{-1}. The asymmetric carboxylate stretching mode of N3|TiO_2 is either absent or too weak to appear near a strong ring stretching band at 1610 cm^{-1}. The C═O stretching mode from the protonated carboxylic acid group was also not observed. In contrast, the spectrum of the free N3 shows a C═O vibration at 1713 cm^{-1} and, as expected, the symmetric carboxylate stretching band at 1388 cm^{-1} was absent as the carboxylic acid groups are fully protonated. The presence of the symmetric carboxylate band at 1388 cm^{-1} in the resonance Raman spectrum of N3|TiO_2 and the lack of a C═O stretching band supports the earlier IR evidence that N3 is bound to TiO_2 nanoparticles via a bridging or bidentate linkage.

Charge-Transfer Dynamics of N3 and N3|TiO_2. Excitation into the ^{1}MLCT of N3 transfers a metal 3d electron to the ligand π^* state, and the excited electron is essentially localized on one of the ligand bipyridine groups.[16,17,44,45,50] This indicates that the excited-state structure of N3 should be similar to that of the N3 radical anion, that is, the radical anion of *cis*-4,4′-dicarboxy-2,2′-bipyridine. The vibrational modes observed in the resonance Raman spectrum provide detailed information about the structural changes associated with the electron transfer. Interestingly, the absolute resonance Raman cross sections of N3|TiO_2 modes are 1.5−2.0 times larger than the corresponding N3 modes, indicating that the TiO_2 surface has a strong affect on the intramolecular charge-transfer dynamics of the adsorbed N3 molecules. The Raman cross section of a mode arising from a resonant electronic transition depends on various factors, the most important ones being the excited-state geometry change (Δ) and the vibrational and electronic dephasing.

Detailed information on the excited-state geometry changes or displacement (Δ) along each vibrational mode can only be obtained from a quantitative analysis of the absolute resonance Raman excitation profiles as performed here. Large displacements are observed for the ring stretching modes, ring breathing, and in-plane ring deformation modes, and they are expected to correspond to lengthening of the bonds in the excited state as the promoted electron occupies an antibonding π^* orbital. For some modes, such as the 1261 and 1310 cm^{-1} bands, the displacements may arise from a decrease of the C−C bond length between the two pyridyl groups of each bipyridyl ligand, similar to the reported bond length decrease and increase in vibrational frequency of inter-ring modes from the normal-coordinate analysis of the ground and excited triplet ^{3}MLCT state of trisbipyridineruthenium(II).[44,45] The bridging Ru−N modes at 318 and 364 cm^{-1} show relatively small displacements, though they connect the donor Ru(II) ion and the acceptor bipyridine ligand, suggesting that the coordinating bonds are largely unaffected by the intramolecular charge transfer. Similar trends were observed for the mode displacements of N3|TiO_2. No modes attributable to TiO_2 were observed in the spectrum. Although we are probing primarily an intramolecular charge transfer, this last result is similar to our earlier study on the heterogeneous charge-transfer dynamics of alizarin adsorbed on the surface of the TiO_2 nanoparticle.

Significant differences in the displacements are seen between the N3 and N3|TiO_2 systems. The Δ's of N3 are larger than the corresponding values for the N3|TiO_2 system, and hence the mode specific reorganization energy of N3 (215 cm^{-1}) is about twice that of N3|TiO_2 (112 cm^{-1}). This result appears counterintuitive, as the Raman cross sections are larger for N3|TiO_2. However, it suggests that other factors, such as electronic dephasing and the binding interaction may play major roles in charge-transfer excited-state dynamics.

In the condensed phase, solvent dynamics may significantly contribute to the breadth of the absorption spectrum,[38−42] through either inhomogeneous or homogeneous mechanisms. The inhomogeneous broadening arises from probing an ensemble of molecules, which have different solvation structures leading to a distribution of electronic transition energies. The inhomogeneous broadening distribution is considered static on the resonance Raman time scale. Homogeneous broadening in the condensed phase is normally dominated by solvent-induced pure electronic dephasing, although population decay also may be important for the N3|TiO_2 complex, due to its sub-100-fs lifetime.[19] The homogeneous broadening for N3 derived from the Brownian oscillator model[31a,40−42] has a line width of 1055 cm^{-1}, while that of N3|TiO_2 (422 cm^{-1}) is a factor of 2.5 less. Thus, the solvent reorganization energy in N3 of 1004 cm^{-1} is about 6 times larger than the value for N3|TiO_2 (161 cm^{-1}). This factor appears to dominate the Raman process in N3 by strongly damping out all of the vibrational modes. It should be noted that the ultrafast ^{1}MLCT relaxation rates of 70 and 30 fs for N3 and N3|TiO_2, respectively, make a significant contribution to the total dephasing rate observed. However, inclusion of this factor only exacerbates the discrepancy in the solvent reorganization energies between free N3 dye and the N3|TiO_2 complex. The larger reorganization energy for free N3 consequently results in their observed lower resonance Raman cross sections and larger Δ's compared to those of N3|TiO_2.

The primary aim of our study is to determine the effect of the TiO_2 nanoparticle on the intramolecular charge-transfer dynamics of the adsorbed N3 dye. The critical parameters in the intramolecular charge-transfer dynamics are, for N3|TiO_2, homogeneous broadening $\Gamma = 422$ cm^{-1}, vibrational reorganization energy $\lambda_v = 112$ cm^{-1}, and solvent reorganization energy $\lambda_s = 161$ cm^{-1}. These values are significantly smaller than those for N3, which has $\Gamma = 1055$ cm^{-1}, $\lambda_v = 215$ cm^{-1}, and $\lambda_s = 1004$ cm^{-1}. The inhomogeneous broadening in N3|TiO_2 ($\Theta = 960$ cm^{-1}) is comparable to that of N3 ($\Theta = 870$ cm^{-1}) and reflects the relative insensitivity of the intramolecular charge transfer to the environment on long time scales. Similarly, the transition moments and zero−zero energies of N3 and N3|TiO_2 are essentially identical, indicating that the electronic properties are the same.

The experimental results and modeling indicate that the effect of the TiO_2 nanoparticle on the adsorbed N3 dye is to reduce

the magnitude of both the vibrational and solvent reorganization energies. A fundamental understanding of the effects of the TiO_2 nanoparticle on the adsorbed N3 may come from the structure of the N3 dye, the surface of the TiO_2 nanoparticle, and their interactions. N3 has two carboxylic acid groups attached to each bipyridine. Due to steric reasons, it has been suggested that N3 uses two of the four carboxylic acid groups to bind to the TiO_2 nanoparticle surface. This binding could substantially rigidify the structure of the adsorbed N3, particularly if two carboxylic acid groups are substituents of the same bipyridine ligand. Increased rigidity of the molecular structure could then lead to the observed smaller Δ's and decreased vibrational reorganization energy for N3|TiO_2 compared to N3. Strong binding could also facilitate subsequent electron injection from the N3 ^{1}MLCT or ^{3}MLCT states into the TiO_2 nanoparticle.

The major effect of TiO_2 on the excited-state dynamics of N3, though, comes from the solvent reorganization energy. The solvent reorganization energy of N3 is 6 times larger than that of N3|TiO_2. This effect could be visualized as arising from either an ensemble or intrinsic property of N3 adsorbed on the surface of the TiO_2 nanoparticle. Our results show that the absolute resonance Raman cross sections are independent of the N3 concentration for both N3|TiO_2 and free N3 systems, indicating that the N3 dye molecules have little interaction with one another. Since absolute resonance Raman cross sections depend on the vibrational and solvent reorganization energies, the effects of TiO_2 on the excited-state dynamics of adsorbed N3 is an intrinsic property of the system and the ensemble property has little or no contributions. The intrinsic property may arise from rapid electronic and vibrational dephasing inside the TiO_2 nanoparticle affecting the dynamics of the adsorbed N3. These processes have been assumed to be responsible for damping out the vibrational modes of the accepting TiO_2 in the alizarin/TiO_2 system.[30] It is nevertheless surprising that adsorption to the TiO_2 nanoparticle surface apparently decreases the solvent reorganization energy by a factor of 6. A number of factors may be responsible for this decrease. A simple decrease in the solvent accessibility of the N3 dye due to physical blocking of solvent molecules by the TiO_2 nanoparticle may lead to a decreased dephasing lifetime and subsequent lower solvent reorganization energy, although the concentration independence of the Raman cross section argues against this factor being significant. A more likely explanation is that the increased rigidity of both the adsorbed dye and solvent near the nanoparticle surface may decrease collision-induced dephasing and, hence, the solvent reorganization energy. It is known that attractive van der Waals forces are much greater near a surface[51] and may effectively result in a layer of "frozen" solvent molecules around the nanoparticle. In the case of TiO_2, this attraction may be enhanced by other attractive interactions, such as dipolar forces, between the TiO_2 oxygens and the surrounding DMSO solvent molecules. An excellent test of this model would be to examine the MLCT dynamics of N3 on TiO_2 in various solvent environments. These experiments are in progress.

The vibrational reorganization energy of N3 obtained in this work is about a factor of ca. 6 smaller than the values reported for similar transition metal complexes by several workers.[52] For example, the total vibrational reorganization energies of $Ru(bpy)_3^{2+}$ and $Fe(bpy)_3^{2+}$ have been estimated to be 1336 and 1345 cm^{-1}, respectively. The reasons for the large discrepancies arise from the assumptions made in the different studies. The researchers in the other studies assumed the validity of the short-time dynamic approximation to extract their values. In the short time limit, the Raman intensities and the excited-state displacements are related by Savin's formula:[53] $I_1/I_2 = (\Delta_1\bar{\nu}_1)^2/(\Delta_2\bar{\nu}_2)^2$, where 1 and 2 refer to two different modes having Raman fundamental intensities I_1 and I_2, frequencies $\bar{\nu}_1$ and $\bar{\nu}_2$, and excited-state displacements Δ_1 and Δ_2, respectively. To obtain the absolute displacement from the relative intensities, this model assumes that the overall width of the absorption spectrum arises entirely from the Franck−Condon progressions and the solvent contribution to the line width merely diffuses the vibronic structure. Finally, in these experiments, the displacements were evaluated from the relative Raman band intensities and not from the absolute Raman cross sections. By ignoring or mimimizing the solvent contribution to the absorption bandwidth, this method may overestimate the excited state displacements and, hence, the vibrational reorganization energy in the condensed phase. Moreover, in these experiments, the Raman intensities are measured at only one/two excitation wavelengths in the post or preresonant region of the absorption spectrum. This procedure can miss any dependence of the intensity on excitation wavelength due to interference from nearby electronic states, even for systems with smooth electronic absorption spectra. Finally, no attempts were made to study overtone or combination intensity to constrain the magnitude of the estimated displacements. Therefore, not surprisingly, the vibrational reorganization energies reported by these workers are similar to the *total* (vibrational and solvent) reorganization energy determined in our experiments. It is interesting to note that the vibrational and solvent reorganization energies obtained for N3 in our experiment are similar to the values reported by Streiff and McHale[54] for $[Ru(NH_3)_4bipyridine]^{2+}$. They used a similar experimental procedure and theoretical model for the absorption and resonance Raman excitation profiles as we used here, to obtain the relevant excited-state parameters such as electronic transition, vibrational, and solvent reorganization energies. The similarity of their values with ours for a similar Ru(II) complex strengthens the validity of the method used in our experiment.

Implications to Photovoltaic Application. The electron-transfer rate from the excited state of N3 adsorbed onto a TiO_2 nanoparticle to the conduction band of the nanoparticle is one of the fastest processes in chemistry.[55,56] A wide variety of dyes, such as porphyrin,[23] phthalocyanine,[57] xanthene,[58] coumarin,[59] and anthraquinone,[33a,60] coupled to TiO_2 nanoparticles have been shown to have electron transfer rates with time constants of

(50) (a) Dallinger, R. F.; Woodruff, W. H. *J. Am. Chem. Soc.* **1979**, *101*, 4391−4393. (b) Bradley, P. G.; Kress, N.; Hornberger, B. A.; Dallinger, R. F.; Woodruff, W. H. *J. Am. Chem. Soc.* **1981**, *103*, 7441−7446.
(51) Hamaker, H. C. *Physica* **1937**, *4*, 1058.
(52) (a) Maruszewski, K.; Bajdor, K.; Strommen, D. P.; Kincaid, J. R. *J. Phys. Chem.* **1995**, *99*, 6286−6293. (a) Doorn, S. K.; Hupp, J. T. *J. Am. Chem. Soc.* **1989**, *111*, 4704−4712. (c) Berger, R. M.; McMillin, D. R. *Inorg. Chim. Acta* **1990**, *177*, 65−69.
(53) Heller, E. J.; Sundberg, R. L.; Tannor, D. *J. Phys. Chem.* **1982**, *86*, 1822−1833.
(54) Streiff, J.; McHale J. L. *J. Chem. Phys.* **2000**, *112*, 841−850.
(55) (a) Zewail, A. H. *Angew. Chem., Int. Ed.* **2000**, *39*, 2586−2631. (b) Diau, E. W.-G.; Herek, J. L.; Kim, Z. H.; Zewail, A. H. *Science* **1998**, *279*, 847−851. (c) Peteanu, L. A.; Schoenlein, R. W.; Wang, Q.; Mathies, R. A.; Shank, C. V. *Proc. Natl. Acad. Sci. U.S.A.* **1993**, *90*, 11762−11766. (d) Owrutsky, J. C.; Li, M.; Locke, B.; Hochstrasser, R. M. *J. Phys. Chem.* **1995**, *99*, 4842−4846. (e) Saito, T.; Kobayashi, T. *J. Phys. Chem. A* **2002**, *106*, 9436−9441.

<100 fs. These rates are significantly faster than those of the homogeneous intramolecular electron-transfer rates with comparable donor−acceptor separation distances,[56] indicating that the TiO_2 nanoparticle has a strong effect on the dynamics of electron transfer. The rate and efficiency of charge separation are critical parameters in the functioning of supramolecular or nanoscale devices (e.g., photoelectrochemical cells based on dye-sensitized TiO_2 nanoparticles). For a photoelectrochemical cell based on N3|TiO_2, charge separation with a time constant of 30 fs has been reported to contribute to 70% of the multicomponent electron-transfer process.[19] The efficiency of the device also critically depends on the charge recombination rate, and for the N3|TiO_2 device, this process is completed in the microsecond to millisecond time scale. Classical electron transfer theory states that for a device to have high efficiency, it should have a small total reorganization energy.[61] The studies presented here show that the intramolecular charge transfer in N3 dye is indeed characterized by a very small reorganization energy. In addition, adsorption onto TiO_2 nanoparticles strongly affects the charge-transfer dynamics and further reduces the total reorganization energy by a factor of ca. 5. Clearly, N3 adsorption onto the TiO_2 nanoparticle renders N3|TiO_2 with superior electron-transfer characteristics for making efficient photovoltaic devices.

(56) (a) Miller, S. E.; Zhao, Y.; Schaller, R.; Mulloni, V.; Just, E. M.; Johnson, R. C.; Wasielewski, M. R. *Chem. Phys.* **2002**, *275*, 167−183. (b) Walker, G. C.; Akesson, E.; Johnson, A. E.; Levinger, N. E.; Barbara, P. F. *J. Phys. Chem.* **1992**, *96*, 3728−3736. (c) Osuka, A.; Noya, G.; Taniguchi, S.; Okada T.; Nishimura, Y.; Yamazaki, I.; Mataga, N. *Chem.—Eur. J.* **2000**, *6*, 33−46.
(57) He, J.; Hagfeldt, A.; Lindquist, S.-E.; Grennberg, H.; Korodi, F.; Sun, L.; Akermark, B. *Langmuir* **2001**, *17*, 2743−2747.
(58) Benko, G.; Hilgendorff, M.; Yartsev, A. P.; Sundstrom, V. *J. Phys. Chem. B* **2001**, *105*, 967−974.
(59) (a) Rehm, J. M.; McLendon, G. L.; Nagasawa, Y.; Yoshihara, K.; Moser, J.; Gratzel, M. *J. Phys. Chem.* **1996**, *100*, 9577−9578. (b) Ghosh, H. N.; Asbury, J. B.; Lian, T. *J. Phys. Chem. B* **1998**, *102*, 6482−6486.
(60) Huber, R.; Moser, J.-E.; Gratzel, M.; Wachtveitl, J. *J. Phys. Chem. B* **2002**, *106*, 6494−6499.
(61) (a) Gao, Y. Q.; Marcus, R. A. *J. Chem. Phys.* **2000**, *113*, 6351−6360. (b) Gosavi, S.; Marcus, R. A. *J. Phys. Chem.* B **2000**, *104*, 2067−2072. (c) Gao, Y. Q.; Georgievskii, Y.; Marcus, R. A. *J. Chem. Phys.* **2000**, *112*, 3358−3369. (d) Ramakrishna, S.; Willig, F.; May, V. *J. Chem. Phys.* **2001**, *115* (6), 2743−2756.

Conclusions

Quantitative modeling of the absorption spectrum and excitation profiles of the Raman fundamentals and overtone bands of free N3 and complexed N3|TiO_2 provided detailed information about the effects of TiO_2 nanoparticles on the intramolecular metal-to-ligand charge-transfer dynamics of the adsorbed N3 dyes. Absorption and resonance Raman spectral studies have provided evidence that N3 dyes are adsorbed on the surface of TiO_2 nanoparticles, and the complex N3|TiO_2 formed is linked via carboxylate bidentate or bridging bonds. The bridge provides weak electronic coupling between N3 and the TiO_2 nanoparticle. Adsorption increases the absolute resonance Raman cross section of each mode by about 1.6 and decreases the mode-specific and solvent reorganization energies by factors of 2 and 6, respectively. Both vibrational and electronic dephasing contribute to the dynamics of electron transfer with the dominant effects originating from the environmental component. The total reorganization energy for N3 is the lowest reported to date and adsorption in N3|TiO_2 further decreases it by a factor of ca. 5. This lowering of the reorganization energy upon adsorption to a TiO_2 nanoparticle may facilitate charge separation and account for the rapid, efficient electron transfer observed in N3|TiO_2.

Acknowledgment. The authors gratefully thank Prof. Anne Myers Kelley for fruitful discussions and for providing the computer program for the time-dependent calculations. The authors thank one of the reviewers for suggesting concentration dependent studies. The authors also acknowledge NSERC Research Grants-in-Aid for providing funding for the work.

Supporting Information Available: Figures showing the resonance Raman spectra of N3 and N3|TiO_2 as a function of excitation wavelength (PDF). This material is available free of charge via the Internet at http://pubs.acs.org.

JA035231V